Heat and Mass Transfer in Inflammation-Induced Glaucoma

applied sciences

MDPI

Article

Heat and Mass Transfer in Inflammation-Induced Glaucoma

Giulia Grisolia [1,*] and Umberto Lucia [2,*]

[1] Dipartimento di Ingegneria dell'Ambiente, del Territorio e delle Infrastrutture, Corso Duca degli Abruzzi 24, 10129 Torino, Italy
[2] Dipartimento Energia "Galileo Ferraris", Politecnico di Torino, Corso Duca degli Abruzzi 24, 10129 Torino, Italy
* Correspondence: giulia.grisolia@polito.it (G.G.); umberto.lucia@polito.it (U.L.); Tel.: +39-011-090-4558 (U.L.)

Abstract

Glaucoma is a complex condition with an unknown exact cause, but it involves progressive damage to the optic nerve. This damage is primarily driven by high eye pressure, poor blood flow, and oxidative stress, a process linked to cell ageing and inflammation that harms the retina. Recent research highlights that these issues stem from structural changes in the eye's drainage system and visual pathways, which can be analysed through the lens of engineering thermodynamics. This study proposes a thermal explanation for the physiological processes linking ocular behaviour to inflammatory ion flux alterations. We develop a thermal model demonstrating that temperature increases are tied to the mechanical work necessary for maintaining water flux in the anterior ocular chamber. We show that these changes alter the membrane potential and tissue pH, resulting in elevated intraocular pressure. By clarifying the temperature–pressure effect, this research establishes a theoretical framework to study the developments of future glaucoma therapies.

Keywords: heat transfer in eyes systems; thermal approach to glaucoma; irreversibility; thermal effects in biosystems; first and second law analysis

1. Introduction

During the last two decades, substantial evidence from animal ocular diseases has shown a relationship between glaucoma disease and eye inflammation [1–5].

Glaucoma is a multifactorial and progressive neurodegenerative ocular diseasem characterized by progressive optic nerve damage and by specific visual field alterations [5,6] due to a progressive loss of retinal ganglionic cells (RGCs) [7] mainly due to mechanical and vascular stress related to hypoxia [8], mitochondrial dysfunction, oxidative stress [9], and neuroinflammation [10]. Glaucoma is also able to cause blindness [5]. Indeed, it represents the cause of approximately 11% of the global population's (aged over 50 years old) blindness [11]. Moreover, an increase from 76.5 million patients in 2020 to an estimated number of 111.8 million patients in 2040 [12] is expected globally.

Elevated intraocular pressure is certainly among the most studied and most relevant risk factors in glaucoma disease because the risk of a visual damage is generally associated with an uncontrolled level of intraocular pressure [13], even if there also exist other non-IOP related factors [14]. Therefore, the actual therapeutic treatment of glaucoma consists of lowering the IOP [15], even if efforts are under development to test antioxidative and immunomodulatory therapies [16].

The cause of the IOP increase is mostly due to aqueous humour resistance to drainage across outflow pathways within the eye. Additionally, oxidative stress generates tissue

Academic Editor: Roberto Zivieri

Received: 28 March 2026
Revised: 13 May 2026
Accepted: 19 May 2026
Published: 22 May 2026

stress with a related activation of local para-inflammation, a mechanism of adaptation that is intermediate between a normal and an inflammatory state [17] but that is useful for maintaining tissue homeostasis and functionality. Dysregulation of para-inflammation causes inflammation (i.e., the primary response of the immune system to infections or tissue injuries [18]) with a release of cytokines and chemokines and related damage to the retina [19] but also an increase in resistance to aqueous outflow in the anterior chamber [20]. Moreover, all living organisms produce reactive oxygen species (ROS) as a by-product of their cellular metabolism [21–23]. While these organisms have antioxidant defences, such as enzymes, proteins, and vitamins, ROS can accumulate due to their overproduction or ineffective antioxidant activity. This accumulation results in a state known as oxidative stress [24]. Ongoing research into the role of ROS in living systems has highlighted their dual effect as activator of a homeostatic compensatory response concerning survival ability and as alleviators or aggregators of the living system's damage, e.g., inflammation [25–27].

Concerning nerves, any stimulus able to cause cell membrane depolarization generates an opening of the voltage-gated Na^+ channels, with a related inflow of small amounts of Na^+, which decreases its electrochemical gradient and depolarises the cell membrane, in turn opening more Na^+ channels up to a value of the Na^+ equilibrium potential of +56 mV. At this state, the cell inactivates the Na^+ channels and opens the voltage-gated K^+ channels [28]. As a consequence of the depolarization, the voltage-gated Ca^{2+} channels are opened, with a release of Ca^{2+} stored in the sarcoplasmic reticulum into the cytosol and the related cell contraction. Moreover, in response to a raised concentration of Ca^{2+} at the cytoplasmic face of the nerve cell membrane, the Ca^{2+}-activated K^+ channel is opened. In the case of membrane depolarization, Mg^{2+} is released; however, if depolarisation occurs together with glutamate binding to the receptor, then the N-methyl-D-aspartate (NMDA) receptor channels (NMDARs), highly permeable to Ca^{2+}, are gated with a great release of glutamate [28].

On the other hand, the channel proteins form gap junctions between two adjacent cells connecting their cytoplasm. Concerning transport efficiency, channels are 10 times more efficient than carriers, allowing more than 10^8 ions s^{-1} to pass through one open channel. On the contrary, channels play a fundamental role only in relation to passive transport, because they cannot be coupled to energy processes (ATP reactions) required for active transport. Consequently, their function concerns the rapid diffusion of some specific inorganic ions, e.g., Na^+, K^+, Ca^{2+}, and Cl^-, caused by electrochemical gradients between the internal and external surface of the cell membrane. Hence, if ion concentrations increase, their flux through a channel increases proportionally up to a saturation level of maximum rate. Moreover, ion channels are not continuously open, but they are gated in response to specific stimuli, e.g., membrane voltage changes, mechanical stresses, and binding of a ligand as extracellular or intracellular mediators, even if many cell's functions require the control of these fluxes [28].

From these considerations, we can highlight that ion transport results in a fundamental aspect for modelling the biophysical mechanisms that cause glaucoma disease. Thus, the biophysical bases of this topic suggest that we should shift our usual perspective by incorporating an engineering thermodynamic and thermal physical approach to analyse fluxes, with particular interest in inflammation [29]. We focus particularly on heat transfer concerning the biochemical work performed by cells in opening and closing their channels [30,31]. Cells are adaptive biological systems that convert chemical energy into work by linking metabolic and biochemical reactions with transport processes. Therefore, this study aims to propose a thermal approach to understand inflammation related to glaucoma. For this purpose, in Section 2, the thermal approach is developed using the first law of thermodynamics and by introducing the Onsager phenomenological equations, which

are useful for linking the macroscopic thermodynamic quantities to the electrochemical quantities of the eye tissues. In Section 3, numerical data are presented together with the related numerical evaluations, which are developed to assess the normal conditions of the eyes; moreover, the link between the thermal and the biophysical quantities is carried out to better understand the biological mechanism of intraocular pressure increase and inflammation. In Section 4, some comments are developed concerning the ion fluxes and the ROS's role in the increase in pressure as a consequence of inflammation.

2. Materials and Methods

Analysing ocular temperature variations under different environmental conditions is essential for understanding both its internal physiology and its interaction with external stimuli. Due to the current lack of experimental facilities for in vivo intraocular temperature measurement, early empirical research was confined to assessing ocular surface temperature [32–34]. Given these experimental constraints, theoretical and numerical simulations have become a primary method for evaluating fluid dynamics and thermal distributions within the eye. Amara [35] utilised a human eye model to investigate the impact of laser power and wavelength on ocular tissues. Bayat et al. [36] utilised 2D and 3D models to study the flow dynamics of partial vitreous liquefaction, treating it as a two-phase viscoelastic Newtonian fluid. Further research by Rahman et al. [37] integrated four physiological age-related variables—metabolism, blood perfusion, tear evaporation, and aqueous humour (AH) flow—to analyse thermo-fluid dynamics. Additionally, Tang et al. [38] simulated flow across diverse morphological structures to map velocity distributions and temperature variations. Moreover, while the sclera is partially exposed to ambient air when the eye is open, existing models often overlook this interaction. Although several studies have investigated the influence of ambient temperature and convection coefficients on ocular thermal variations, they often fail to correlate these coefficients with specific environmental conditions [32].

The complexity of the human eye arises from the interdependent relationship between thermal, fluid, and mechanical stressors. Because the flow of aqueous humour modulates intraocular pressure—a critical factor in tissue health—accurate multi-physics computational models are required to map these interactions. Effective modelling necessitates the integration of thermal regulation and fluid–structure interaction to capture the organ's physiological response. These predictive tools can be categorized by their methodology: top–down strategies, which utilize *in vivo* parameter estimation, or bottom–up approaches, which rely on mechanistic parameters to forecast concentration profiles [39].

2.1. The Physiological Bases for the Thermophysical Model: Fluid-Dynamic Considerations

The aqueous humour, secreted by the ciliary body, is a clear intraocular fluid that circulates from the posterior to the anterior chamber. Its subsequent drainage via the trabecular meshwork and uveoscleral routes is a primary determinant of intraocular pressure (IOP). Beyond the pressure gradients established by AH secretion and outflow, the fluid's behaviour is affected by gravitational orientation and thermal gradients, specifically the convective currents arising from the temperature differential between the core body temperature and the cooler corneal surface. Adopting the methodology of Abdelhafid et al. [40] and Wang et al. [41,42], this model treats the AH as an incompressible Newtonian fluid. Furthermore, the Boussinesq approximation is usually applied, wherein density fluctuations are ignored in all instances except for the buoyancy term, providing a simplified framework for analysing thermally driven flow [39].

2.2. The Physiological Bases for the Thermophysical Model: Thermal Considerations

In healthy populations, central corneal surface temperatures typically fluctuate between 32 °C and 36 °C [43]. Research indicates a centripetal thermal gradient; temperatures rise progressively from the corneal apex toward the periphery [44]. Specifically, the limbal region is approximately 0.45 °C to 1.0 °C warmer than the center [45]. This disparity is attributed to the lack of corneal vasculature and the cooling effects of continuous tear film evaporation at the center. In static air, a linear correlation exists between environmental and corneal temperatures; for instance, every 1 °C increase in room temperature corresponds to a 0.15 °C to 0.20 °C rise in ocular surface temperature (OST) [46]. Conversely, lower ambient temperatures and increased air velocity serve to depress OST [47], while relative humidity appears to have a negligible impact [48]. The integrity of the tear film is a critical determinant of OST [45]. Patients with dry eye syndrome often exhibit lower corneal temperatures and accelerated cooling rates compared to healthy controls [49]. Furthermore, blinking introduces dynamic thermal shifts [33]; the action restores the tear film and brings the ocular surface into contact with the vascularized palpebral conjunctiva, momentarily raising the OST toward core body temperatures [33]. Upon eye opening, rapid cooling occurs, with healthy subjects showing an average decrease of 0.24 °C in the first second [50]. Mydriasis has been associated with an average corneal temperature increase of 0.82 ± 0.13 °C and higher heat flux density [43]. This may occur because the iris, characterized by low blood flow, otherwise acts as a thermal barrier between the choroid and the anterior chamber [43]. OST strongly mirrors systemic body temperature, with a 1 °C increase in core temperature resulting in a nearly equivalent 0.98 °C rise in OST [48]. While interocular temperature differences are generally negligible, with 95% of the population showing a difference of $\leq$0.60 °C [51], significant diurnal variations exist. Temperatures typically peak in the afternoon, tracking the body's natural circadian rhythm [52]. Advancing age correlates with a decline in OST, estimated at a reduction of 0.010 °C to 0.023 °C per year [43]. Comparative studies show that individuals in their sixth decade exhibit central corneal temperatures approximately 1 °C lower than those in their twenties: this age-related cooling and the accompanying reduction in heat flux density are likely secondary to choroidal atrophy and diminished ocular blood flow [43].

2.3. The Physiological Bases for the Thermophysical Model: Scaling Considerations

The intraocular fluid dynamics within the anterior chamber are characterized by a single convection cell, with buoyant ascent occurring near the posterior boundary and descent occurring along the anterior wall. Lateral fluid velocity is negligible, suggesting a predominantly two-dimensional flow field. Empirical observations indicate typical transit times of approximately 60 s, the duration required for a fluid particle to traverse from the superior to the inferior pole. The aqueous humour is continuously secreted by the ciliary body, entering the chamber via the pupillary aperture [53].

2.4. The Thermophysical Approach

In this section, we develop a thermodynamic model. It is based on the following assumption, derived from previous physiological evidence. For the purposes of this model, the medium is treated as a Newtonian fluid, with physical properties equivalent to those of water. Outflow occurs via the trabecular meshwork located at the iridocorneal angle. This convective flow is driven by a trans-corneal temperature gradient. The posterior boundary of the chamber is maintained near core body temperatures, whereas the external corneal surface is exposed to ambient conditions. Given a constant corneal thickness and thermal conductivity comparable to water, the temperature of the internal corneal endothelium

remains slightly below core temperatures. In this framework, we must consider only average values of the physical quantities (pressure, density, *etc.*).

IOP is generated and maintained by water inflows and outflows between the ocular anterior chamber and blood vessels. Thus, by introducing a thermodynamic approach, we can consider the eye as an open system, for which the first law of thermodynamics can be written as follows [50]:

$$\begin{aligned}\dot{Q} - \dot{W} = \frac{d}{dt}\left(U + p_0\, V + \int_V \rho\,(e_k + e_{pot})\, dV\right)_{CV} + \\ + \dot{m}_{out}\,(h + e_k + e_{pot})_{out} - \dot{m}_{in}\,(h + e_k + e_{pot})_{in}\end{aligned} \tag{1}$$

where $\dot{Q}$ is the heat rate exchanged between the cornea and its environment; $\dot{W}$ is the mechanical power exhibited by the tissue concerning pressure and the cornea's elastic properties; t is the time; U is the internal energy; p_0 is the environmental pressure; V is the volume of the anterior chamber; ρ is the water density; $\dot{m}$ is the water's mass flow rate; e is the specific energy; k and pot stand for kinetic and potential, respectively; h is the water's specific enthalpy; in and out stand for inflow and outflow respectively; CV means control volume. The kinetic energy and potential energy variations can be neglected, because their magnitudes are negligible relative to the enthalpy components, and the system is analysed in stationary conditions so that it follows

$$\dot{Q} - \dot{W} = \dot{m}_{out}\, h_{out} - \dot{m}_{in}\, h_{in} \tag{2}$$

where the specific enthalpy concerns the under-cooling state of water [54]:

$$h(T) = h_{sat}(T) + v_{sat}(T) \cdot \big(p - p_{sat}(T)\big) \tag{3}$$

where $h_{sat}(T)$ is the water's saturation enthalpy at temperature T, $p_{sat}(T)$ is the water's saturation pressure at temperature T, $v_{sat}(T)$ is the water's saturation specific volume at the temperature T, and p is the working pressure.

From Equation (2), it is possible to evaluate the work done by the eye system to maintain the normal condition, i.e., IOP $= p = (16 \pm 2)$ mmHg [55,56]. Of course, in that case, we expect to obtain a range of normal behaviour.

The mechanical power generated is the (mechanical and electrochemical) work of the tissue cells' membranes. In order to model this process, we can consider the Onsager phenomenological equations [57–61]:

$$\begin{cases} \mathbf{J}_e = -L_{11}\,\dfrac{\nabla\phi}{T} - L_{12}\,\dfrac{\nabla T}{T^2} \\ \\ \mathbf{J}_Q = -L_{21}\,\dfrac{\nabla\phi}{T} - L_{22}\,\dfrac{\nabla T}{T^2} \end{cases} \tag{4}$$

where $\mathbf{J}_e$ depicts the current density [A m^{-2}], $\mathbf{J}_Q$ stands for the heat flux [W m^{-2}], ϕ is the membrane electric potential, T is the living cell temperature, L_{ij} denotes the phenomenological coefficients such that $L_{12} = L_{21}$ in the absence of magnetic fields and $L_{11} \geq 0$, $L_{22} \geq 0$, and $L_{11}L_{22} - L_{12}^2 > 0$ [57–63]: L_{11} and L_{22} represent heat conductivity and electrical conductivity, respectively, while L_{12} and L_{21} are cross-coefficients independent of both L_{11}

and L_{22} [62,63]. These relations, in the approximation of constant temperature, become the following:

$$\begin{cases} \mathbf{J}_e = -L_{11}\,\dfrac{\nabla\phi}{T} \\ \\ \mathbf{J}_Q = -L_{21}\,\dfrac{\nabla\phi}{T} \end{cases} \tag{5}$$

Consequently,

$$\mathbf{J}_e = \frac{L_{11}}{L_{21}}\,\mathbf{J}_Q \Rightarrow \nabla\cdot\mathbf{J}_e = \frac{L_{11}}{L_{21}}\,\nabla\cdot\mathbf{J}_Q \tag{6}$$

Now, considering that

$$\int_V \nabla\cdot\mathbf{J}_Q\,dV = \dot{Q} \tag{7}$$

it follows that

$$\int_V \nabla\cdot\mathbf{J}_e dV = \frac{L_{11}}{L_{21}}\int_V \nabla\cdot\mathbf{J}_Q\,dV = \frac{L_{11}}{L_{21}}\,\dot{Q} \tag{8}$$

which means that the result of any thermal perturbation (inflammation in our analysis) can not only be converted in ion fluxes but also that every ion flux causes heat flux. In this study, we have introduced the Onsager equations only to highlight the effects that thermal perturbations can have on the electrochemical response and vice versa, without using them for any numerical evaluation. This work does not aim to provide an exhaustive examination of the Onsager theory itself. Rather, our analysis is developed within the context of a biophysical framework. For comprehensive details on the Onsager theory, readers are referred to the original papers in Refs. [62,63]. Thus, this approach points out the relationship between the previous introduced distinct biophysical phenomena. To evaluate them, we consider the accepted approach to the living cell membrane based on the effects of ion fluxes, which, in turn, change the membrane electric potential; therefore, the cell must restore its normal membrane electric potential by generating counter-fluxes. Indeed, the electric membrane potential can be expressed as follows:

$$\begin{aligned} nZF\,\Delta\phi &= \Delta H_{memb} - \dot{Q}\,\tau + 2.3\,RT_0\,\Delta(\mathrm{pH}) = \\ &= \Delta H_{memb} - \left(\dot{W} + \dot{m}_{out}\,h_{out} - \dot{m}_{in}\,h_{in}\right)\tau + 2.3\,RT_0\,\Delta(\mathrm{pH}) \end{aligned} \tag{9}$$

where ϕ denotes the tissue cells' electric membrane potential; ΔH_{memb} is the enthalpy variation of the tissue cells' membrane system; $\dot{Q}$ stands for the heat flow; τ represents the characteristic time of the process; n is the number of moles of ions considered; R and F are the universal ideal gas and the Faraday constants, respectively; T_0 is the environmental temperature of the cell; Z is the ion valence; ΔpH is the variation of the pH inside the tissue. In particular, these electric processes generate biochemical phenomena: Na^+, K^+, and Cl^- ion fluxes determine membrane voltage regulation, while Ca^{2+} and Mg^{2+} ion fluxes control protein folding; Zn^{2+} controls HCO^{3-} formation; Fe^{2+} activates molecular oxygen and works as a catalyst for the generation of ROS in pathological conditions such as inflammation, carcinogenesis, and perfusion injury.

3. Results

In this work, we focus and analyse eye inflammation using the first principle of thermodynamics. To this purpose, first, we must evaluate the normal range of biophysical quantities related to the eyes.

Concerning the thermal properties of water, we consider the usual *thermodynamic properties tables* in engineering thermodynamics reported in Ref. [54]; for biophysical properties,

we refer to Refs. [64,65]; regarding the thermal properties of eyes, we consider the results summarised in Ref. [66].

To solve Equation (2), first, we evaluate the enthalpies of water inflow and outflow using Equation (3).

The water inflow temperature T_{in} is assumed to be equal to the artery temperature of 36.7 °C [66], while the water outflow temperature T_{out} is assumed to be the eye's anterior chamber temperature of (30.7 ± 1.7) °C [64]. In stationary and healthy conditions, water flows result in $\dot{V}_{in} = \dot{V}_{out} = (2.25 \pm 0.75)$ µL min^{-1} [41]. The ocular anterior chamber volume is $V = (171.4 \pm 42.4)$ µL [65].

Concerning water inflow, we introduce the hypotheses usually accepted in medicine, i.e., temperature and pressure of inflowing water are the same of blood:

- Pressure Range: $p \in [80, 120]$ mmHg $\approx$ [10,666, 15,999] Pa, with a mean value evaluated as follows [67]:

$$p_{av} = p_{min} + \frac{p_{max} - p_{min}}{3} = 93.3 \text{ mmHg} \approx 93 \text{ mmHg} = 12{,}443 \text{ Pa} \quad (10)$$

  where $p_{min} = 80$ mmHg and $p_{max} = 120$ mmHg are the minimum and maximum value of blood pressure considered in healthy conditions, and p_{av} is its mean value, the pressure with respect to which we have evaluated the subsequent thermodynamic quantities;
- Water density results in 994.5 kg m^{-3}, obtained by interpolation of the values in the range $t \in [25.0, 40.0]$°C, considering that the inflow water is at a temperature of 36.7 °C and the outflow water is at 30.7 °C [54];
- Water Mass Flow: $\dot{m} = \rho \dot{V} \approx (3.73 \pm 1.24) \times 10^{-8}$ kg s^{-1}, where $\dot{V} = \dot{V}_{in} = \dot{V}_{out}$
- The water's specific enthalpy evaluated using Equation (3) and the table of water properties in Ref. [54]:
  - Inflow: Value at inflow mean pressure (93 mmHg) of $h_{av,in} = 153.75$ kJ kg^{-1};
  - Outflow: Value at inflow mean pressure (93 mmHg) and in the temperature range (30.7 ± 1.7) °C, with $h_{av,out} = 128.67$ kJ kg^{-1} at its central value;
- Water enthalpy rate evaluated as $\dot{H} = dH/dt = \dot{m}\, h_{av}$, as published in Ref. [54]:
  - Inflow: $\dot{H} = \dot{m}_{in}\, h_{av,in} = (5.73 \pm 1.91)$ mW;
  - Outflow: $\dot{H} = \dot{m}_{out}\, h_{av,out} = (4.81 \pm 1.60)$ mW.

Concerning Equation (2), we can calculate the enthalpy rate variation as $\dot{m}_{out}\, h_{out} - \dot{m}_{in}\, h_{in} = -(0.92 \pm 0.31)$ mW.

Now, we must evaluate the heat exchanged by the eye. To achieve this, we consider the approach followed in Ref. [66] but for a stationary state for eyes, corresponding to a normal mean behaviour of the eyes themselves. Thus, we consider the electric equivalence [54] for the cornea, and we introduce its thermal properties:

- Corneal Thermal Conductivity: $\lambda = 0.580$ W m^{-1} °C^{-1};
- Corneal Convective Coefficient: $\alpha = 14$ W m^{-2} °C^{-1};
- Emissivity: $\varepsilon = 0.975$;
- The minimum temperature of the cornea external surface was experimentally measured, and it can be set at $T_c \approx (34.30 \pm 0.07)$°C [68];
- Following Pennes' approach for the bioheat equation [69], the temperature of the cornea's internal surface is set to T_{out};
- The ambient temperature is chosen at $T_0 = 25$°C$= 298.15$ K.

The heat power can be evaluated as follows:

$$\dot{Q} = \dot{Q}_{cond} + \dot{Q}_{conv} + \dot{Q}_{rad} \quad (11)$$

where $\dot{Q}_{cond} = \lambda\, A\, (T_c - T_{out})/(r_{ext} - r_{int})$, with $r_{int} = 6.8$ mm being the average cornea internal radius and $r_{ext} = 7.2$ mm being the average cornea external radius. Then, $\dot{Q}_{conv} = \alpha\, A\, (T_0 - T_c)$ and $\dot{Q}_{rad} = \sigma\, (T_0^4 - \varepsilon\, T_c^4)\, A$ [54], and $\sigma = 5.67 \times 10^{-8}$ W m^{-2} K^{-4} is the Stefan–Boltzmann constant [54], $A = (1.3 - 1.4)$ cm^2 is the area of the surface of the cornea, and d is its thickness. The conductive heat power must be considered in relation to the cornea's geometry.

To do so, we approximate the cornea as a part of a sphere, so we evaluate the thermal conductive resistance for the cap of a hollow sphere. For that purpose, we consider the thermal flux as follows:

$$\dot{Q}_{cd} = -\lambda\, \Omega\, r^2\, \frac{dT}{dr} \tag{12}$$

where Ω is the solid angle at the center of the sphere cap, determined by considering that the cap area is $A \approx 1.35$ cm^2 $= 1.35 \times 10^{-4}$ m^2 in relation to a radius of $r_{ext} = 7.2 \times 10^{-3}$ m, obtaining $\Omega = A/r_{ext}^2 = 2.60$ sr. From Equation (12), it follows that

$$\dot{Q}_{cd} = -\lambda\, \Omega \left(\frac{1}{r_{ext}} - \frac{1}{r_{int}} \right)^{-1} (T_c - T_{out}) = 665.6 \text{ mW} \tag{13}$$

The convective flux results in $\dot{Q}_{cv} = -17.6$ mW, while the radiative flux results in $\dot{Q}_{rad} = -6.2$ mW. Consequently, the net heat flux results in $\dot{Q} = 641.8$ mW. We highlight that the conductive heat transfer is the dominant effect over convection, radiation, and flow rate enthalpy variation. For future experimental use of the model, this approach could be simplified by considering only conductive heat transfer with a deviation of 3.6% based on the difference between 665.6 mW and 642.7 mW.

From the first principle (Equation (2)), the chemical and mechanical power developed to maintain a stationary state for the eye at a normal pressure of (16 ± 2) mmHg results in $\dot{W} = \dot{Q} - \dot{m}_{out}\, h_{out} + \dot{m}_{in}\, h_{in} = 642.7$ mW. This power is required to overcome the mechanical friction of water flows and to maintain the ion fluxes in the tissue cells for their work. Recently, we have developed an analysis of inflammation in the context of pain, showing that when inflammation occurs, temperature changes with a related variation in heat flux and entropy rate, with a consequent variation in mechanical power too.

In Figure 1, mechanical power, evaluated using Equation (2), is represented as a function of the temperature of water outflow. We highlight that mechanical power decreases with temperature growth (inflammation state). This can be interpreted as a related demand of energy from the tissue cells in order to maintain normal pressure conditions. Moreover, we consider the Gibbs free energy variation:

$$dG = -dW = V\, dp - S\, dT + \sum_i \mu_i\, dN_i \tag{14}$$

where G is the Gibbs free energy; W is the work; V is the volume; p is the pressure (IOP—intraocular pressure in this study); S is the entropy; T is the temperature; μ_i is the chemical potential of the i-th chemical species; N_i is the number of particles that flow across of the boundary of the system. It follows that in isothermal conditions ($dT = 0$) with constant ion flux (i.e., stationary inflammation state), every decrease in mechanical work causes an increase in pressure.

Now, from Equation (14), by introducing the definition of the electrochemical potential for a living cell membrane, i.e., the Gibbs free energy density [70] for a cell membrane,

$$\tilde{\mu} = \frac{G}{V} = F\, \Delta\phi - 2.3\, RT\, \Delta\text{pH} \tag{15}$$

and the definition of membrane electric potential elementary variation in relation to the ion concentration,

$$d\phi = -\frac{RT}{ZF}\frac{dc}{c} \tag{16}$$

we can obtain the following relation:

$$dp = -\frac{RT}{ZV}\frac{dc}{c} - \sum_i \frac{\mu_i}{V} dN_i - 2.3\frac{RT}{V} d\mathrm{pH} \tag{17}$$

This last equation related the pressure variation with the pH changes in the eye and the flux of the involved ions. Some numerical results previously evaluated in Ref. [30] are summarised in Table 1.

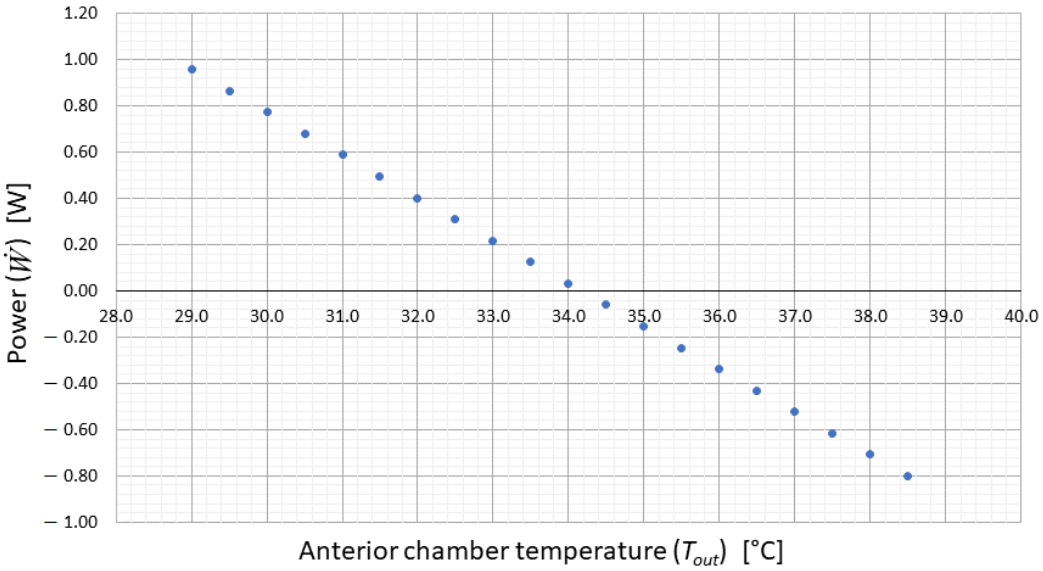

Figure 1. Mechanical power related to water inflow and outflow is a function of outflow temperature (Equation (2)). The shape of the mechanical power line highlights that it decreases with an increase in temperature (inflammation). Consequently, energy is demanded from the tissue to maintain normal pressure conditions.

Table 1. Pressure drop evaluation of Equation (17) on the basis of Cl^- fluxes across the ciliary body or ciliary epithelium, as summarized in Reference [71].

Species	Net Fluxes [mol s^{-1} m^{-2}]	Pressure Drop [mmHg]
Cat	8.03×10^{-6}	±6.1
Toad	7.23×10^{-6}	±5.4
Rabbit	6.26×10^{-6}	±4.7
Bovine	2.86×10^{-6}	±2.1

In order to compare our results with the experimental ones, we consider that the ion concentration can be evaluated as follows:

$$c_f = c_i - \frac{r_p \cdot \dot{n} \cdot A\, t}{V} \tag{18}$$

where c_f is the concentration after the intraocular pressure variation; c_i is the concentration before the intraocular pressure variation; r_p is the intraocular pressure ratio, $\dot{n}$ is the ion

flux; V is the eye's anterior chamber volume; $A = 1.04 \pm 0.12$ cm^2 is the cornea's surface; t is the time during which the intraocular pressure variations occur.

As a case study, we consider the rabbit eye. Concerning rabbits, our results can be compared with the experimental ones reported in Ref. [72], and they are summarised in Table 2. We evaluate c_f and compare them with the measured values, as reported in Table 2. The concentration c_i before the intraocular pressure variation can be obtained by the experimental results reported in Table 2; r_p is the ratio between the intraocular variation (obtained considering the values in Table 2) and the value obtained in Table 1 (pressure drop), where the value of $\dot{n}$ is reported for rabbits: $t = 35$ min as reported in Ref. [72] and $V = 0.29$ mL as reported in Ref. [73]. The comparison is reported in Table 3 by considering the pressure drop evaluated using Equation (17) on the basis of Cl^- fluxes through the ciliary body or ciliary epithelium. This table shows an agreement between our theoretical results and the experimental ones from the literature, with an error in the range of [3.1, 19.0] with a mean error of 10%. We highlight that our results depend on the initial values. The initial values used in our simulation are the ones of Ref. [72], so our results are affected by the inhomogeneous behaviour of the eyes in relation to the expected Cl^- concentration that varies in the range of [3.0, 16.0]%. Moreover, we are not able to evaluate whether our confidence interval agrees with the experimental one, because the data collected in the literature were reported without the error range.

Table 2. Concentration of chloride, sodium, and potassium (mEq L^{-1}) in aqueous humour and intraocular pressure (IOP mmHg) of rabbits before the induced ion-concentration reduction and after 35 min of the induced ion reduction, as summarized in Reference [72].

Concentration			IOP	
Cl^-	Na^+	K^+	OD	OS
[mEq L^{-1}]	[mEq L^{-1}]	[mEq L^{-1}]	[mmHg]	[mmHg]
Before concentration reduction				
110	161	4.60	18.86	20.55
113	155	4.60	18.86	20.55
101	141	4.48	20.55	18.86
99	133	4.35	17.30	18.86
99	135	3.90	18.86	20.55
100	147	4.60	17.30	17.30
104	138	4.86	18.86	18.86
98	141	4.48	20.55	20.55
104	138	5.12	18.86	17.30
After concentration reduction				
100	133	5.12	10.24	11.20
103	138	5.24	14.57	10.24
94	133	4.22	10.24	10.24
96	141	5.63	8.54	9.36
84	114	4.22	10.24	8.54
84	110	4.22	9.36	10.24
108	143	4.35	9.36	9.36
87	122	4.82	10.24	11.20
91	127	4.10	7.10	7.79

Table 3. Comparison between our results and the experimental ones reported in Reference [72].

Pressure Ratio r_p	Related Cl^- Flux $\dot{n}$	Cl^- Concentration Calculated Final $c_{f,calc}$	Cl^- Concentration Measured Final $c_{f,meas}$	Percentage Error Δc_f%
[adim]	[mmol h^{-1} cm^{-2}]	[mmol L^{-1}]	[mmol L^{-1}]	[%]
9.00×10^{-4}	2.02×10^{-6}	110.00	100	10.0
7.31×10^{-4}	1.64×10^{-6}	113.00	103	9.7
1.35×10^{-3}	3.05×10^{-6}	100.99	94	7.4
3.05×10^{-3}	6.86×10^{-6}	98.99	96	3.1
6.89×10^{-4}	1.55×10^{-6}	99.00	84	17.9
4.69×10^{-4}	1.06×10^{-6}	100.00	84	19.0
-2.38×10^{-3}	-5.35×10^{-6}	104.01	108	−3.7
8.95×10^{-4}	2.01×10^{-6}	98.00	87	12.6
8.19×10^{-4}	1.84×10^{-6}	104.00	91	14.3

4. Discussion

Glaucoma is a progressive multifactorial neuropathy that affects the optic system by inducing retinal ganglion cell apoptosis and optic disc cupping [74]. Thus, it introduces damage to the optic nerve and retinal nerve fibre layer. After cataracts, it is the major cause of blindness worldwide, and in most cases, it is detected only once visual damage is widely declared (partial vision loss). Elevated values of IOP remain a key determinant for assessing glaucoma progression, and being the sole known modifiable risk factor, the IOP is the one targeted by glaucoma treatments.

Within the eye, the role of the aqueous humour is to maintain stable intraocular pressure at normal values, as well as maintaining the shape of the eyeball. The ciliary body produces the aqueous humour, which percolates across the posterior chamber, at the border of the lens, and by the pupil, exiting through the semiporous trabecular meshwork (iridocorneal angle of the anterior chamber); therefore, it flows into the Schlem canal and passes through the distal collector channels, leaving the eye. Finally, it is drained into the venous system. The insufficient drainage of the aqueous humour (due to higher resistance through the trabecular meshwork or to the occlusion of the angle, or both) is included within the pathogenesis of glaucoma. Both causes of insufficient drainage results in an increase in the IOP, which in turn leads to progressive and irreversible neuropathy, resulting in ganglion cell apoptosis [75].

Moreover, secretion of aqueous humour is physiologically important because it provides nutrients and oxygen to the avascular anterior segment and sustains inflation of the globe, ensuring normal visual function; today, reducing the secretory rate to lower intraocular pressure is a major strategy in treating glaucomatous patients [71]. The non-pigmented cell represents the site of solute and water efflux into the posterior aqueous chamber [76], and the mechanisms are mediated by the Na/K-ATPase, which is localised to the basolateral membrane of non-pigmented cells [77]. Due to this active pumping by the Na/K-ATPase, the intracellular potassium concentration is high. As a consequence of the electrochemical gradient, the Cl^- ions leave the non-pigmented cells and pass into the posterior chamber [76]. Membrane hyperpolarisation increases the driving force for Cl^- ion efflux [77]. The mechanisms and regulation of anion transport are important in understanding aqueous humour formation, but Cl^- is the anion of crucial importance [71]. The Na^+/H^+ exchanger mediates sodium entry into the pigmented cells, while the Cl/HCO_3 exchanger is responsible for Cl^- ion entry. These exchangers are independent, even if they are physiologically coupled via carbonic anhydrase [77].

In particular, these electric processes generate different biochemical phenomena: Na^+, K^+, and Cl^- ion fluxes determine membrane voltage regulation, while Ca^{2+} and Mg^{2+} ion fluxes control protein folding; Zn^{2+} controls HCO^{3-} formation, and Fe^{2+} activates molecular oxygen and works as a catalyst for the generation of ROS in pathological conditions, such as inflammation [78,79], carcinogenesis, and perfusion injury.

Our results are consistent with prior experimental studies. Indeed, the volume inside trabecular meshwork cells is controlled by the intracellular Na-K-Cl cotransport system. Some experimental evidence suggests that the volume of trabecular meshwork cells affects the permeability of the trabecular meshwork itself [80]. A decrease in outflow facility through the trabecular meshwork is believed to be the main reason for high intraocular pressure in primary open-angle glaucoma. This implies that the function of the Na-K-Cl cotransport system may change in glaucomatous trabecular meshwork cells compared to normal trabecular meshwork cells [80,81]. Researchers studied the activity of the Na-K-Cl cotransport system in monolayers of trabecular meshwork cells, which was measured as ouabain-insensitive and bumetanide-sensitive K. They found that the Na-K-Cl cotransport activity in glaucomatous trabecular meshwork cells was $(32 \pm 2)\%$ lower than in normal trabecular cells [81]. Additionally, Western blot analyses revealed that the expression of cotransporter proteins in glaucomatous trabecular meshwork cells was reduced by $(64 \pm 14)\%$ compared to normal trabecular cells [81]. As a result, it is proven that the function and regulation of Na-K-Cl cotransport are altered in glaucomatous trabecular meshwork cells compared to normal ones. However, despite reduced Na-K-Cl cotransport activity, the observation that the cell volume of glaucomatous trabecular meshwork cells is greater than that of normal trabecular cells suggests that other pathways for ion flux, involved in the regulation of cell volume, may play a role in the reduced outflow of glaucoma [80,81].

The thermodynamic approach developed here allows us to link all the biophysical evidence to an analytical model for the comprehension of the processes involved, linking macroscopic to microscopic results and vice versa. Indeed, our analytical results allow us to show how the temperature increase (inflammation) is able to determine pressure growth. On the other hand, this pressure increase is also related to ion fluxes (Equation (17)) through the Gibbs' equation. The thermodynamic approach allows the comprehension of how persistent ocular inflammation can induce glaucoma.

Specifically,the trabecular meshwork outflow pathways play a crucial role in regulating the drainage of the aqueous humour, thereby controlling intraocular pressure. The structure of these pathways and the level of resistance they offer seem to be influenced by the contraction of the ciliary muscle and the cells of the scleral spur. The scleral spur contains axons that either innervate the scleral spur cells or exhibit characteristics similar to mechanosensory nerve endings [82]. In this context, chloride (Cl^-) ions are the primary anions transported across the epithelium through chloride channels [83]. This process is related to the Na-K-Cl cotransport mechanism. Furthermore, experimental observations have shown that variations in corneal temperature are correlated with changes in blood flow [84–86] and in IOP [87,88]. Consequently, it is believed that both oxidative stress and the stimulation of sympathetic nerve fibres due to temperature fluctuations can influence the regulation of aqueous humour vortex flow and turnover, thus impacting IOP values [88].

5. Conclusions

Our results represent an engineering thermodynamic approach to an open problem in a particular biosystem, the eye, concerning the pathology of glaucoma. Our results agree with studies on morphological changes in the trabecular meshwork (TM) that have

been observed through transmission electron microscopy. In human TM tissues from patients with primary open-angle glaucoma (POAG), significant immunoreactivity for cytokines IL-6, IL-1β, and TNF-α was noted when compared to control subjects, suggesting that these cytokines may be associated with disease activity. Indeed, TM endothelial cells secrete various factors and cytokines that modulate the functions of the cells and the extracellular matrix (ECM) within the conventional outflow pathway. In the context of glaucoma, macrophages in the TM produce cytokines such as IL-6, IL-1β, and TNF-α, which trigger an acute inflammatory response and recruit additional immune cells, including T lymphocytes. Furthermore, TGF-β1 regulates and promotes the expression of IL-6 in the TM, which can indirectly induce angiogenesis by stimulating the expression of vascular endothelial growth factor (VEGF). These findings not only support both previous evidence suggesting that growth factors and cytokines can induce ECM remodelling and alter cytoskeletal interactions in the TM but also support the engineering thermodynamics results that represent a theoretical explanation of this process.

Thus, the result obtained represents an improvement in the comprehension of this pathology that could allow us to develop potential anti-inflammatory and antioxidant strategies able to support present anti-glaucoma therapies.

Author Contributions: Conceptualisation, U.L. and G.G.; methodology, U.L.; validation, U.L. and G.G.; formal analysis, U.L.; investigation, U.L. and G.G.; resources, U.L.; data curation, G.G.; writing—original draft preparation, U.L. and G.G.; writing—review and editing, U.L. and G.G.; visualization, G.G.; supervision, U.L.; project administration, U.L.; funding acquisition, U.L. All authors have read and agreed to the published version of the manuscript.

Funding: This research received no external funding.

Institutional Review Board Statement: Not applicable.

Informed Consent Statement: Not applicable.

Data Availability Statement: All data used in this research were obtained from the literature cited within the text.

Conflicts of Interest: The authors declare no conflicts of interest.

References

1. Naskar, R.; Wissing, M.; Thanos, S. Detection of Early Neuron Degeneration and Accompanying Microglial Responses in the Retina of a Rat Model of Glaucoma. *Investig. Ophthalmol. Vis. Sci.* **2002**, *43*, 2962–2968.
2. Bosco, A.; Steele, M.R.; Vetter, M.L. Early microglia activation in a mouse model of chronic glaucoma. *J. Comp. Neurol.* **2011**, *519*, 599–620. https://doi.org/10.1002/cne.22516.
3. Sapienza, A.; Raveu, A.L.; Reboussin, E.; Roubeix, C.; Boucher, C.; Dégardin, J.; Godefroy, D.; Rostène, W.; Reaux-Le Goazigo, A.; Baudouin, C.; et al. Bilateral neuroinflammatory processes in visual pathways induced by unilateral ocular hypertension in the rat. *J. Neuroinflamm.* **2016**, *13*, 44. https://doi.org/10.1186/s12974-016-0509-7.
4. Oikawa, K.; Ver Hoeve, J.N.; Teixeira, L.B.C.; Snyder, K.C.; Kiland, J.A.; Ellinwood, N.M.; McLellan, G.J. Sub-region-Specific Optic Nerve Head Glial Activation in Glaucoma. *Mol. Neurobiol.* **2020**, *57*, 2620–2638. https://doi.org/10.1007/s12035-020-01910-9.
5. Baudouin, C.; Kolko, M.; Melik-Parsadaniantz, S.; Messmer, E.M. Inflammation in Glaucoma: From the back to the front of the eye, and beyond. *Prog. Retin. Eye Res.* **2021**, *83*, 1000916. https://doi.org/10.1016/j.preteyeres.2020.100916.
6. Weinreb, R.N.; Aung, T.; Medeiros, F.A. The pathophysiology and treatment of glaucoma: A review. *J. Am. Med. Assoc.* **2014**, *311*, 1901–1911. https://doi.org/10.1001/jama.2014.3192.
7. Ventura, L.M.; Sorokac, N.; Santos, R.D.L.; Feuer, W.J.; Porciatti, V. The Relationship between Retinal Ganglion Cell Function and Retinal Nerve Fiber Thickness in Early Glaucoma. *Investig. Ophthalmol. Vis. Sci.* **2006**, *47*, 3904. https://doi.org/10.1167/iovs.06-0161.
8. Harris, A.; Rechtman, E.; Siesky, B.; Jonescu-Cuypers, C.; McCranor, L.; Garzozi, H.J. The role of optic nerve blood flow in the pathogenesis of glaucoma. *Ophthalmol. Clin. N. Am.* **2005**, *18*, 345–353. https://doi.org/10.1016/j.ohc.2005.04.001.

9. Osborne, N.N.; Núñez-Álvarez, C.; Del Olmo-Aguado, S.; Merrayo-Lloves, J. Visual light effects on mitochondria: The potential implications in relation to glaucoma. *Mitochondrion* **2017**, *36*, 29–35. https://doi.org/10.1016/j.mito.2016.11.009.
10. Jiang, S.; Kametani, M.; Chen, D.F. Adaptive immunity: New aspects of pathogenesis underlying neurodegeneration in glaucoma and optic neuropathy. *Front. Immunol.* **2020**, *11*, 65. https://doi.org/10.3389/fimmu.2020.00065.
11. Steinmetz, J.D.; Bourne, R.R.A.; Briant, P.S.; Flaxman, S.R.; Taylor, H.R.B.; Jonas, J.B.; Abdoli, A.A.; Abrha, W.A.; Abualhasan, A.; Abu-Gharbieh, E.G.; et al. Causes of blindness and vision impairment in 2020 and trends over 30 years, and prevalence of avoidable blindness in relation to VISION 2020: The Right to Sight: An analysis for the Global Burden of Disease Study. *Lancet Glob. Health* **2021**, *9*, 144–160. https://doi.org/10.1016/s2214-109x(20)30489-7.
12. Tham, Y.C.; Li, X.; Wong, T.Y.; Quigley, H.A.; Aung, T.; Cheng, C.Y. Global prevalence of glaucoma and projections of glaucoma burden through 2040: A systematic review and meta-analysis. *Ophthalmology* **2014**, *121*, 2081–2090. https://doi.org/10.1016/j.ophtha.2014.05.013.
13. Kooner, K. Risk factors for progression to blindness in high tension primary open angle glaucoma: Comparison of blind and nonblind subjects. *Clin. Ophthalmol.* **2008**, *2*, 757–762. https://doi.org/10.2147/opth.s3139.
14. Tejwani, S.; Dinakaran, S.; Mehta, P.; Mehta, R.; Tilva, B.; Arora, D. Significance of non-intraocular pressure (IOP)-related factors particularly in normal tension glaucoma: Looking beyond IOP. *Indian J. Ophthalmol.* **2022**, *70*, 569. https://doi.org/10.4103/ijo.ijo_861_21.
15. Shields, M.B. Normal-tension glaucoma: Is it different from primary open-angle glaucoma? *Curr. Opin. Ophthalmol.* **2008**, *19*, 85–88. https://doi.org/10.1097/icu.0b013e3282f3919b.
16. Buonfiglio, F.; Pfeiffer, N.; Gericke, A. Immunomodulatory and Antioxidant Drugs in Glaucoma Treatment. *Pharmaceuticals* **2023**, *16*, 1193. https://doi.org/10.3390/ph16091193.
17. Xu, H.; Chen, M.; Forrester, J.V. Para-inflammation in the aging retina. *Prog. Retin. Eye Res.* **2009**, *28*, 348–368. https://doi.org/10.1016/j.preteyeres.2009.06.001.
18. Retamal, M.A.; Bennett, M.V.L.; Pelegrin, P.; Fernandez, R. Ion Channels in Inflammatory Processes: What Is Known and What Is Next? *Mediat. Inflamm.* **2016**, *2016*, 6245731. https://doi.org/10.1155/2016/6245731.
19. Chen, M.; Muckersie, E.; Forrester, J.V.; Xu, H. Immune activation in retinal aging: A gene expression study. *Investig. Ophthalmol. Vis. Sci.* **2010**, *51*, 5888–5896. https://doi.org/10.1167/iovs.09-5103.
20. Saccà, S.C.; Pulliero, A.; Izzotti, A. The dysfunction of the trabecular meshwork during glaucoma course. *J. Cell. Physiol.* **2015**, *230*, 510–525. https://doi.org/10.1002/jcp.24826.
21. Pontes Oliveira de Almeida, A.J.; Pinheiro Lúcio de Oliveira, J.C.; da Silva Pontes, L.V.; de Souza Júnior, J.F.; Felisberto Gonçalves, T.A.; Dantas, S.H.; de Almeida Feitosa, M.S.; Silva, A.O.; de Medeiros, I.A. ROS: Basic Concepts, Sources, Cellular Signaling, and its Implications in Aging Pathways. *Oxidative Med. Cell. Longev.* **2022**, *2022*, 225578. https://doi.org/10.1155/2022/1225578.
22. Schieber, M.; Chandel, N.S. ROS function in redox signaling and oxidative stress. *Curr. Biol.* **2014**, *24*, R453–R462. https://doi.org/10.1016/j.cub.2014.03.034.
23. Sies, H.; Belousov, V.V.; Chandel, N.S.; Davies, M.J.; Jones, D.P.; Mann, G.E.; Murphy, M.P.; Yamamoto, M.; Winterbourn, C. Defining roles of specific reactive oxygen species (ROS) in cell biology and physiology. *Nat. Rev. Mol. Cell Biol.* **2022**, *23*, 499–515. https://doi.org/10.1038/s41580-022-00456-z.
24. Sies, H.; Berndt, C.; Jones, D.P. Oxidative Stress. *Annu. Rev. Biochem.* **2017**, *86*, 715–748. https://doi.org/10.1146/annurev-biochem-061516-045037.
25. Lapointe, J.; Hekimi, S. When a theory of aging ages badly. *Cell. Mol. Life Sci.* **2010**, *67*, 1–8. https://doi.org/10.1007/s00018-009-0138-8.
26. Hekimi, S.; Lapointe, J.; Wen, Y. Taking a "good" look at free radicals in the aging process. *Trends Cell Biol.* **2011**, *21*, 569–576. https://doi.org/10.1016/j.tcb.2011.06.008.
27. Liguori, I.; Russo, G.; Curcio, F.; Bulli, G.; Della-Morte, L.A.D.; Gargiulo, G.; Testa, G.; Cacciatore, F.; Bonaduce, D.; Abete, P. Oxidative stress, aging, and diseases. *Clin. Interv. Aging* **2018**, *13*, 757–772. https://doi.org/10.2147/CIA.S158513.
28. Alberts, B.; Johnson, A.; Lewis, J.; Raff, M.; Roberts, K.; Walter, P. *Molecular Biology of the Cell*, 4th ed.; Garland Science: New York, NY, USA, 2002.
29. Lucia, U.; Grisolia, G.; Ponzetto, A.; Deisboeck, T.S. Thermophysical Insights into the Anti-Inflammatory Potential of Magnetic Fields. *Biomedicines* **2024**, *12*, 2534. https://doi.org/10.3390/biomedicines12112534.
30. Lucia, U.; Grisolia, G.; Astori, M.R. Constructal law analysis of Cl^- transport in eyes aqueous humor. *Sci. Rep.* **2017**, *7*, 6856. https://doi.org/10.1038/s41598-017-07357-8.
31. Lucia, U.; Grisolia, G.; Dolcino, D.; Astori, M.R.; Massa, E.; Ponzetto, A. Constructal approach to bio-engineering: The ocular anterior chamber temperature. *Sci. Rep.* **2016**, *6*, 31099.
32. Feyli, F.; Yaghoubi, M.; Ahmadi, G.; Abouali, O. Thermal Energy Removal From a Human Eye for Different Environmental Conditions—A Computational Fluid Dynamics Study Using a Full-Scale Mannequin. *ASME Open J. Eng.* **2025**, *4*, 041035. https://doi.org/10.1115/1.4070015.

33. Mapstone, R. Determinants of corneal temperature. *Br. J. Ophthalmol.* **1968**, *52*, 729–741. https://doi.org/10.1136/bjo.52.10.729.
34. Mapstone, R. Ocular thermography. *Br. J. Ophthalmol.* **1970**, *54*, 751–754. https://doi.org/10.1136/bjo.54.11.751.
35. Amara, E.H. Numerical investigations on thermal effects of laser-ocular media interaction. *Int. J. Heat Mass Transf.* **1995**, *38*, 2479–2488. https://doi.org/10.1016/0017-9310(94)00353-w.
36. Bayat, J.; Emdad, H.; Abouali, O. Numerical investigation of partially liquefied vitreous dynamics as two-phase viscoelastic-Newtonian fluid flow in a planar cavity due to oscillatory motion. *Int. J. Multiph. Flow* **2020**, *127*, 103259. https://doi.org/10.1016/j.ijmultiphaseflow.2020.103259.
37. Rahman, M.A.; Rabbani, M.; Maruf, M.H.; Islam, A.; Shihavuddin, A.S.M. Characterizing the Aging Process of the Human Eye: Tear Evaporation, Fluid Dynamics, Blood Flow, and Metabolism-Based Comparative Study. *BioMed Res. Int.* **2022**, *2022*, 805402. https://doi.org/10.1155/2022/2805402.
38. Tang, H.; Qin, Z.; Wen, B. Geometric Model and Numerical Study of Aqueous Humor Hydrodynamics in the Human Eye. *Comput. Math. Methods Med.* **2022**, *2022*, 4756728. https://doi.org/10.1155/2022/4756728.
39. Saigre, T.; Chabannes, V.; Prud'homme, C.; Szopos, M. Mathematical Modeling and Simulation of Coupled Aqueous Humor Flow and Temperature Distribution in a Realistic 3D Human Eye Geometry. *Int. J. Numer. Methods Biomed. Eng.* **2026**, *42*, e70132. https://doi.org/10.1002/cnm.70132.
40. Abdelhafid, F.; Guidoboni, G.; Okumura, N.; Koizumi, N.; Srinivas, S.P., Operator Splitting for the Simulation of Aqueous Humor Thermo-Fluid-Dynamics in the Anterior Chamber. In *Recent Developments in Mathematical, Statistical and Computational Sciences*; Springer International Publishing: Berlin/Heidelberg, Germany, 2021; pp. 489–499. https://doi.org/10.1007/978-3-030-63591-6_45.
41. Wang, W.; Qian, X.; Song, H.; Zhang, M.; Liu, Z. Fluid and structure coupling analysis of the interaction between aqueous humor and iris. *BioMedical Eng. OnLine* **2016**, *15*, 133. https://doi.org/10.1186/s12938-016-0261-3.
42. Dvoriashyna, M.; Pralits, J.O.; Tweedy, J.H.; Repetto, R., Mathematical Models of Aqueous Production, Flow and Drainage. In *Ocular Fluid Dynamics*; Springer International Publishing: Berlin/Heidelberg, Germany, 2019; pp. 227–263. https://doi.org/10.1007/978-3-030-25886-3_9.
43. Zadorozhnyy, O.S.; Korol, A.R.; Naumenko, V.O.; Pasyechnikova, N.V.; Butenko, L.L. Heat exchange in the human eye: A review. *J. Ophthalmol.* **2022**, *6*, 50–58. https://doi.org/10.31288/oftalmolzh202265058.
44. Kamao, T.; Yamaguchi, M.; Kawasaki, S.; Mizoue, S.; Shiraishi, A.; Ohashi, Y. Screening for Dry Eye With Newly Developed Ocular Surface Thermographer. *Am. J. Ophthalmol.* **2011**, *151*, 782–791.e1. https://doi.org/10.1016/j.ajo.2010.10.033.
45. Haber-Olguin, A.; Polania-Baron, E.J.; Trujillo-Trujillo, F.; Graue Hernandez, E.O. Thermographic Behavior of the Cornea During Treatment With Two Excimer Laser Platforms. *Transl. Vis. Sci. Technol.* **2021**, *10*, 27. https://doi.org/10.1167/tvst.10.9.27.
46. Purslow, C.; Wolffsohn, J.S.; Santodomingo-Rubido, J. The effect of contact lens wear on dynamic ocular surface temperature. *Contact Lens Anterior Eye* **2005**, *28*, 29–36. https://doi.org/10.1016/j.clae.2004.10.001.
47. Tan, J.H.; Ng, E.Y.K.; Rajendra Acharya, U.; Chee, C. Infrared thermography on ocular surface temperature: A review. *Infrared Phys. Technol.* **2009**, *52*, 97–108. https://doi.org/10.1016/j.infrared.2009.05.002.
48. Rysä, P.; Sarvaranta, J. Corneal temperature in man and rabbit: Observations made using an infra-red camera and a cold chamber. *Acta Ophthalmol.* **1974**, *52*, 810–816. https://doi.org/10.1111/j.1755-3768.1974.tb01117.x.
49. Petznick, A.; Tan, J.H.; Boo, S.K.; Lee, S.Y.; Acharya, U.R.; Tong, L. Repeatability of a New Method for Measuring Tear Evaporation Rates. *Optom. Vis. Sci.* **2013**, *90*, 366–371. https://doi.org/10.1097/opx.0b013e318288bdd1.
50. Bejan, A. *Shape and Structure, from Engineering to Nature*; Cambridge University Press: Cambridge, UK, 2000.
51. Koçak, I.; Orgül, S.; Flammer, J. Variability in the Measurement of Corneal Temperature Using a Noncontact Infrared Thermometer. *Ophthalmologica* **1999**, *213*, 345–349. https://doi.org/10.1159/000027452.
52. Refinetti, R. Circadian rhythmicity of body temperature and metabolism. *Temperature* **2020**, *7*, 321–362. https://doi.org/10.1080/23328940.2020.1743605.
53. Canning, C.R.; Dewynne, J.; Fitt, A.D.; Greaney, M.J. Fluid flow in the anterior chamber of a human eye. *Math. Med. Biol.* **2002**, *19*, 31–60. https://doi.org/10.1093/imammb/19.1.31.
54. Çengel, Y.; Boles, M.; Kanoğlu, M. *Themodynamics: And Engineering Approach*; McGraw-Hill: New York, NY, USA, 2019.
55. Lucia, U.; Grisolia, G. Thermal Physics and Glaucoma: From Thermodynamic to Biophysical Considerations to Designing Future Therapies. *Appl. Sci.* **2020**, *10*, 7071. https://doi.org/10.3390/app10207071.
56. Grisolia, G.; Astori, M.; Ponzetto, A.; Vercesi, A.; Lucia, U. Thermal Physics and Glaucoma II: Preliminary Evidences for a Thermophysical Design of a Possible Visible-Light-Photons Therapy. *Appl. Sci.* **2021**, *11*, 6301. https://doi.org/10.3390/app11146301.
57. Yourgrau, W.; van der Merwe, A.; Raw, G. *Treatise on Irreversible and Statistical Thermophysics*; Dover: New York, NY, USA, 1982.
58. Callen, H.B. *Thermodynamics*; Wiley: New York, NY, USA, 1960.
59. Katchalsky, A.; Currant, P.F. *Nonequilibrium Thermodynamics in Biophysics*; Harvard University Press: Boston, MA, USA, 1965.

60. Demirel, Y.; Sandler, S.I. Nonequilibrium Thermodynamics in Engineering and Science. *J. Phys. Chem. B* **2004**, *108*, 31–43.
61. Lucia, U.; Grisolia, G. How Life Works — A Continuous Seebeck-Peltier Transition in Cell Membrane? *Entropy* **2020**, *22*, 960. https://doi.org/10.3390/e22090960.
62. Onsager, L. Reciprocal relations in irreversible processes: I. *Phys. Rev.* **1931**, *37*, 405–426.
63. Onsager, L. Reciprocal relations in irreversible processes: II. *Phys. Rev.* **1931**, *38*, 2265–2279.
64. Shinoda, K.; Yagura, K.; Matsumoto, S.; Terauchi, G.; Mizota, A.; Miyake, Y. Intraocular Temperature at Different Sites in Eye Measured at the Beginning of Vitreous Surgery. *J. Clin. Med.* **2021**, *10*, 3412. https://doi.org/10.3390/jcm10153412.
65. Labiris, G.; Gkika, M.; Katsanos, A.; Fanariotis, M.; Alvanos, E.; Kozobolis, V. Anterior chamber volume measurements with Visante optical coherence tomography and Pentacam: Repeatability and level of agreement. *Clin. Exp. Ophthalmol.* **2009**, *37*, 772–774. https://doi.org/10.1111/j.1442-9071.2009.02132.x.
66. Cvetković, M.; Peratta, A.; Poljak, D. Exposed To Infrared Radiation Of 1064 Nm Nd:YAG And 2090 Nm Ho:YAG Lasers. In *Environmental Health Risk V*; Brebbia, C.A., Ed.; WIT Press: Southapmpton, UK, 2009; pp. 221–231. https://doi.org/10.2495/EHR090221.
67. Feher, J. 5.9 - Vascular Function: Hemodynamics. In *Quantitative Human Physiology*; Feher, J., Ed.; Academic Press: Boston, MA, USA, 2012; pp. 498–507. https://doi.org/10.1016/B978-0-12-382163-8.00054-2.
68. Efron, N.; Young, G.; Brennan, N.A. Ocular surface temperature. *Curr. Eye Res.* **1989**, *8*, 901–906.
69. Pennes, H.H. Analysis of Tissue and Arterial Blood Temperatures in the Resting Human Forearm. *J. Appl. Physiol.* **1948**, *1*, 93–122. https://doi.org/10.1152/jappl.1948.1.2.93.
70. Atkins, P.; Paula, J.D. *Physical Chemistry for Life Sciences*; Oxford University Press: New York, NY, USA, 2006.
71. Do, C.W.; Civan, M.M. Basis of Chloride Transport in Ciliary Epithelium. *J. Membr. Biol.* **2004**, *200*, 1–13. https://doi.org/10.1007/s00232-004-0688-5.
72. Ramos, L.; Ramos, A.O.; Giesbrecht, A.M. Changes of Intraocular Pressure and of Chloride, Sodium and Potassium Concentrations in Aqueous Humor and Serum of Rabbits Following Ethanol. *Ophthalmologica* **1969**, *159*, 430–435. https://doi.org/10.1159/000305940.
73. Watsky, M.A.; Jablonski, M.M.; Edelhauser, H.F. Comparison of conjunctival and corneal surface areas in rabbit and human. *Curr. Eyes Res.* **1988**, *7*, 483–486. https://doi.org/10.3109/02713688809031801.
74. Kang, J.M.; Tanna, A.P. Glaucoma. *Med Clin. North Am.* **2021**, *105*, 493–510. https://doi.org/10.1016/j.mcna.2021.01.004.
75. Wagner, I.V.; Stewart, M.W.; Dorairaj, S.K. Updates on the Diagnosis and Management of Glaucoma. *Mayo Clin. Proc. Innov. Qual. Outcomes* **2022**, *6*, 618–635. https://doi.org/10.1016/j.mayocpiqo.2022.09.007.
76. Wiederholt, M.; Helbig, H.; Korbmacher, C. Ion transport across the ciliary epithelium: Lessons from cultured cells and proposed role of the carbonic anhydrase. In *Carbonic Anhydrase*; Botre, F.; Gross, G.; Storey, B.T., Eds.; VCH Weinheim: New York, NY, USA, 1991.
77. To, C.H.; Do, C.W. Ion transport mechanisms in the formation of aqueous humor. *Hong Kong J. Ophthalmol.* **1998**, *2*, 35–42.
78. Taurone, S.; Ripandelli, G.; Pacella, E.; Bianchi, E.; Plateroti, A.M.; De Vito, S.; Plateroti, P.; Grippaudo, F.R.; Cavallotti, C.; Artico, M. Potential regulatory molecules in the human trabecular meshwork of patients with glaucoma: Immunohistochemical profile of a number of inflammatory cytokines. *Mol. Med. Rep.* **2014**, *11*, 1384–1390. https://doi.org/10.3892/mmr.2014.2772.
79. Vernazza, S.; Tirendi, S.; Bassi, A.M.; Traverso, C.E.; Saccà, S.C. Neuroinflammation in Primary Open-Angle Glaucoma. *J. Clin. Med.* **2020**, *9*, 3172. https://doi.org/10.3390/jcm9103172.
80. Al-Aswad, L.A.; Gong, H.; Lee, D.; O'Donnell, M.E.; Brandt, J.D.; Ryan, W.J.; Schroeder, A.; Erickson, K.A. Effects of Na-K-2Cl Cotransport Regulators on Outflow Facility in Calf and Human Eyes In Vitro. *Investig. Ophthalmol. Vis. Sci.* **1999**, *40*, 1695–1701.
81. Putney, L.K.; Brandt, J.D.; O'Donnell, M.E. Na-K-Cl cotransport in normal and glaucomatous human trabecular meshwork cells. *Investig. Ophthalmol. Vis. Sci.* **1999**, *40*, 425–434.
82. Tamm, E.R. The trabecular meshwork outflow pathways: Structural and functional aspects. *Exp. Eye Res.* **2009**, *88*, 648–655. https://doi.org/10.1016/j.exer.2009.02.007.
83. Goel, M.; Picciani, R.G.; Lee, R.K.; Bhattacharya, S.K. Aqueous humor dynamics: A review. *Open Ophthalmol. J.* **2010**, *4*, 52–59. https://doi.org/10.2174/1874364101004010052.
84. Sodi, A.; Giambene, B.; Falaschi, G.; Caputo, R.; Innocenti, B.; Corvi, A.; Menchini, U. Ocular Surface Temperature in Central Retinal Vein Occlusion: Preliminary Data. *Eur. J. Ophthalmol.* **2007**, *17*, 755–759. https://doi.org/10.1177/112067210701700511.
85. Galassi, F.; Giambene, B.; Corvi, A.; Falaschi, G. Evaluation of ocular surface temperature and retrobulbar haemodynamics by infrared thermography and colour Doppler imaging in patients with glaucoma. *Br. J. Ophthalmol.* **2007**, *91*, 878–881. https://doi.org/10.1136/bjo.2007.114397.
86. Auker, C.R. Choroidal Blood Flow: I. Ocular Tissue Temperature as a Measure of Flow. *Arch. Ophthalmol.* **1982**, *100*, 1323. https://doi.org/10.1001/archopht.1982.01030040301020.

87. Leshno, A.; Stern, O.; Barkana, Y.; Kapelushnik, N.; Singer, R.; Prat, D.L.; Cohen, G.; Ben-David, G.; Abrahami, D.; Huna-Baron, R.; et al. Ocular surface temperature differences in glaucoma. *Eur. J. Ophthalmol.* **2021**, *32*, 1518–1524. https://doi.org/10.1177/11206721211023723.
88. Fabiani, C.; Li Voti, R.; Rusciano, D.; Mutolo, M.G.; Pescosolido, N. Relationship between Corneal Temperature and Intraocular Pressure in Healthy Individuals: A Clinical Thermographic Analysis. *J. Ophthalmol.* **2016**, *2016*, 3076031. https://doi.org/10.1155/2016/3076031.